Role of Eddy Forcing in the Dynamics of Multiple Zonal Jets in a Model of the North Atlantic

IGOR KAMENKOVICH

Rosenstiel School of Marine and Atmospheric Science, University of Miami, Miami, Florida

PAVEL BERLOFF*

Woods Hole Oceanographic Institution, Woods Hole, Massachusetts, and Department of Applied Mathematics and Theoretical Physics, University of Cambridge, Cambridge, United Kingdom

JOSEPH PEDLOSKY

Woods Hole Oceanographic Institution, Woods Hole, Massachusetts

ABSTRACT

Multiple zonal jets are observed in satellite data–based estimates of oceanic velocities, float measurements, and high-resolution numerical simulations of the ocean circulation. This study makes a step toward understanding the dynamics of these jets in the real ocean by analyzing the vertical structure and dynamical balances within multiple zonal jets simulated in an eddy-resolving primitive equation model of the North Atlantic. In particular, the authors focus on the role of eddy flux convergences (''eddy forcing'') in supporting the buoyancy and relative/potential vorticity (PV) anomalies associated with the jets. The results suggest a central role of baroclinic eddies in the barotropic and baroclinic dynamics of the jets, and significant differences in the effects of eddy forcing between the subtropical and subpolar gyres. Additionally, diabatic potential vorticity sources and sinks, associated with vertical diffusion, are shown to play an important role in supporting the potential vorticity anomalies. The resulting potential vorticity profile does not resemble a ''PV staircase''—a distinct meridional structure observed in some idealized studies of geostrophic turbulence.

1. Introduction and background

Our view of the ocean circulation is changing continually. The original depiction of the ocean circulation as a steady, large-scale flow has advanced to a much more complex picture with motions and variability on a wide range of spatial and temporal scales. One of the examples of the recent advances in our understanding of the ocean circulation is a discovery of multiple predominantly zonal jets. These zonal jets have been observed in

the time-averaged anomalies of the geostrophic velocity estimated from altimeter data (Maximenko et al. 2005; Sokolov and Rintoul 2007; Huang et al. 2007). These jets correspond to zonal currents with the direction alternating with latitude and speeds of several centimeters per second. The meridional width of these flow patterns is approximately 150–300 km in midlatitudes, and the zonal extent is comparable to the width of the ocean basin they populate. Identification of these jets with in situ observations is challenging because of often poor horizontal and temporal resolution, but there are several observational studies that report the existence of the jets in various parts of the World Ocean. In particular, narrow zonal currents, with direction alternating in latitude, were detected in float measurements in the Brazil basin of the deep South Atlantic (Treguier et al. 2003; Hogg and Owens 1999), equatorial Atlantic (Ollitrault et al. 2006), and in the Southern Ocean (Nowlin and Klinck 1986; Orsi et al. 1995).

* Additional affiliation: Department of Mathematics and Grantham Institute for Climate Change, Imperial College, London, United Kingdom.

Corresponding author address: Igor Kamenkovich, Division of MPO, Rosenstiel School of Marine and Atmospheric Science, University of Miami, 4600 Rickenbacker Causeway, Miami, FL 33149.
E-mail: ikamenkovich@rsmas.miami.edu

The mechanisms of formation and maintenance of the jets are still under debate, and differing views have been proposed in idealized studies with quasigeostrophic (QG) systems (e.g., Rhines 1975). Many of these theories consider dynamical balances in the QG potential vorticity (PV) and argue for the central role of mesoscale eddies in the jet dynamics. In the pioneering work on the subject, Rhines (1975) introduced the idea that the meridional structure of the barotropic jets is maintained by the balance between advections of the relative and planetary vorticity, leading to a distinct meridional scale (i.e., Rhines scale). Panetta (1993), in his study of the doubly periodic, two-layer, baroclinically unstable eastward flow, describes the formation of the jets driven by the converging eddy fluxes of the relative vorticity. Panetta (1993) finds the jet meridional scale to be consistent with the Rhines scale (in the explored parameter regime) and reports the asymmetry between the faster and narrower eastward jets and the weaker and broader westward jets. These results are extended toward the wind-forced, two- and three-layer channel model in Treguier and Panetta (1994). Thompson and Young (2007) emphasize the importance of baroclinic–barotropic interactions and the role of bottom friction. Berloff et al. (2009a, hereafter referred to as BKPa) demonstrate that the formation of baroclinic zonal jets is a result of the instability of transient meridional jets, or "noodle modes." Such modes are, in turn, products of the baroclinic instability of background zonal flow. The accompanying linear stability analysis performed at different stages of this multistep formation process further confirms these conclusions. There are also indications that the jet formation can be influenced by nonlocal mechanisms, involving interactions of linear modes (Berloff 2005a; Kramer et al. 2006).

Several studies attempt to bring insight into this problem by describing the jet formation kinematically. Dritschel and McIntire (2008) and Baldwin et al. (2007) describe the jet structure as the tendency of a flow to form the so-called potential vorticity staircase—the meridional PV profile characterized by alternating broad regions of weak and narrow regions of sharp PV gradients. The underlying idea of this conjecture is the existence of narrow material transport barriers that are associated with the eastward jets; these meandering barriers separate regions with intense eddy PV mixing, associated with the westward jets. The existence of the perfect "PV staircase" is, however, not confirmed by several studies of the oceanic jets (e.g., Panetta 1993; Huang and Robinson 1998; Berloff et al. 2009b, hereafter referred to as BKPb). Instead, the term "PV washboard" (BKPb) seems more appropriate for the description of the meridional PV structure.

A different approach is adapted in studies that describes the process of the barotropic zonal jet formation as an anisotropic inverse cascade of kinetic energy from isotropic mesoscale eddies to multiple zonal currents (Vallis and Maltrud 1993; Galperin et al. 2004; Danilov and Gurarie 2004; Danilov and Gryanik 2004)—the so-called spectral energy cascade theories. Nadiga (2006) further suggests the role that free Rossby waves play in arresting the inverse cascade of energy. Both the PV staircase and spectral energy cascade theories are based on idealized *barotropic* models and do not address the baroclinic dynamics of the jets.

The relevance of the above theories and highly idealized models to the real ocean remains unclear. A step in this direction is to describe the phenomenology of the jets and to find corresponding dynamical balances in the real ocean, focusing on the role of eddies in these balances. While observation-based analysis of jet dynamics is problematic because of the lack of data, numerical eddy-resolving simulations offer complete sets of data. Several studies document the existence of zonal jets in comprehensive eddy-resolving numerical simulations of the North Pacific (Masumoto et al. 2004; Nakano and Hasumi 2005; Richards et al. 2006). The simulated jets resemble the observations at the surface and populate the oceans all the way to the bottom. In this study, we analyze the role of barotropic and baroclinic eddies in the dynamics of the jets in a primitive equation model of the North Atlantic of intermediate complexity. Although our model retains some realistic features of the North Atlantic circulation, the model includes idealizations, which are intended to make calculations possible and to simplify the analysis.

The task of identifying the role of eddies in the near-equilibrium state has to rely on the analysis of the eddy flux convergences. These convergences can be tentatively interpreted as internally generated *eddy forcing* that maintains or resists the jetlike anomalies in, for example, the vorticity and buoyancy equations. The action of the eddy forcing is balanced by the dynamical terms that depend on the mean fields, such as advection and dissipation of the mean vorticity and buoyancy. It is this balance that determines the structure of the jets. In our interpretation of the eddy forcing structure in this study, we assume that a significant *positive* spatial correlation of the eddy forcing with vorticity/buoyancy anomalies implies that this forcing acts to *support* these anomalies and thus the jets themselves [see, e.g., Panetta (1993) for a similar approach]. Although such an approach is not rigorous when a steady state is considered, it can be supported by the following argument: in a steady state, such "in phase" eddy forcing is balanced by terms negatively correlated with the vorticity/

buoyancy anomalies. A removal of this in phase eddy forcing would thus result in a time tendency in the vorticity/buoyancy equation that acts to weaken the jets. The in phase eddy forcing in a steady state can, therefore, be interpreted as supporting the jets. By a similar argument, a negative correlation of eddy forcing with the jetlike anomalies implies that the forcing acts to resist the jets. Note, however, that even strong positive correlation does not imply causality, and cannot explain jet formation.

The eddies discussed in this manuscript are defined as fluctuations from long-term time means, and do not necessarily correspond to short spatial scales. In fact, in order for eddy forcing to be strongly spatially correlated with jetlike anomalies, its dominant meridional scale has to be the same as the jet width. The eddies with the meridional scale comparable to the jet width can thus be expected to play an important role in the jet dynamics. BKPa indeed demonstrate the central role of unstable baroclinic modes with the spatial scale of several Rossby deformation radii.

The paper is organized as follows: the numerical model is described in section 2. Section 3 describes the phenomenology of the zonal jets. We begin by describing the baroclinic structure of the velocities (section 3a). The balances for the density and the relative and potential vorticities are described in the rest of section 3, with a particular focus on the structure of eddy forcing and on the relative importance of the barotropic and baroclinic dynamics. Conclusions are drawn in section 4.

2. Model

The numerical model used in this study is based on the Geophysical Fluid Dynamics Laboratory (GFDL) Modular Ocean Model (MOM) 3.0 code (Pacanowski and Griffies 1999), which solves the equations of motion on fixed geopotential surfaces. The horizontal resolution is 1/8° in both latitudinal and longitudinal directions, which resolves the first Rossby deformation radius. The model domain spans the North Atlantic region from 14° to 60°N and from 70° to 10°W. The depth of the ocean is limited to 3000 m, which roughly corresponds to the depth of the North Atlantic Deep Water cell in the real ocean (Talley 2003). There are 30 vertical levels with thicknesses increasing away from the surface. Model topography is estimated from the 1° × 1° Scripps dataset.

Boundary conditions are identical to those in a 10-layer version of this model in Booth and Kamenkovich (2008). The surface heat and freshwater fluxes have a form of restoration to the annual-mean climatological values of the sea surface temperature and salinity, both derived from the high-resolution (1/4°) analyses of the

World's Oceans, version 2 (Boyer et al. 2005). The restoring time scales for temperature and salinity are 60 and 180 days (for a 50-m mixed layer), respectively. The annual-mean zonal, τ^x, and meridional, τ^y, components of the surface wind stress are derived from the National Centers for Environmental Prediction (NCEP) 1979–2001 reanalysis. Special care was taken to avoid steplike structures in the wind stress curl: the fields on the original coarse grid were smoothed and then interpolated to the model grid by using bicubic splines. The model solves for the explicit free-surface evolution. Sponge boundaries, where the temperature and salinity are restored to the annual-mean climatology with the time scale of 180 days, are employed at the northern and southern boundaries of the domain in order to mimic buoyancy exchanges with the ocean outside the model domain. Solid insulating walls are placed at the eastern and western boundaries. The boundary conditions do not impose any variability on the flow, and all the resulting eddy variability is, therefore, intrinsic. Although the restoring conditions at the surface will shorten the lifetime of surface buoyancy anomalies, the restoring time scale (60 days for temperature) is long enough for the mesoscale variability on the time scale of several weeks.

Most of horizontal mixing of momentum, temperature, and salinity is done by explicitly simulated mesoscale eddies. Small horizontal viscosity and diffusion is retained in the model in order to represent submesoscale mixing processes and for the sake of numerical stability [biharmonic horizontal viscosity and diffusivity is 10^{11} m^4 s^{-1} and 10^{10} m^4 s^{-1}, respectively; see also Smith et al. (2000) who use similar values]. The viscosity corresponds to the viscous boundary layer of 0.25° (at 30°N)—the minimum zonal scale resolved in the model. The diffusivity coefficient used was found to effectively prevent bolus numerical dispersion of tracers in the model. Vertical diffusion is kept to a realistically low value for the ocean above rough topography—10^{-5} m^2 s^{-1} (Ledwell et al. 1993). Thus, the explicit diapycnal mixing in the model is smaller than a typical value used in most numerical models of the ocean circulation, but closer to reality.[1] A quadratic bottom stress of the form $c_{bot}|\mathbf{u}|\mathbf{u}$ was used with the coefficient $c_{bot} = 0.001$ [see Smith et al. (2000) for a nearly identical choice of bottom friction]. Vertical viscosity is 10^{-4} m^2 s^{-1}.

It is common practice to analyze numerical solutions with stratification in a near-equilibrium state, which

---

[1] The amount of bolus numerical diffusivity is hard to estimate accurately but is expected to be of the same or even smaller order than the explicit diffusion (Griffies and Hallberg 2000).

requires adequate spinup time. Among the physical processes determining the oceanic stratification, the slowest process is the vertical diffusion of heat and salt. Taking advantage of the fact that vertical diffusive fluxes do not depend on the horizontal resolution explicitly, we use the method of accelerated convergence that employs a series of simulations with increasing horizontal resolution. First, the $1° \times 1°$ version of the model was spun up from rest for 2000 yr. The resulting ocean state was interpolated to a $\frac{1}{2}° \times \frac{1}{2}°$ grid and then used to initialize the $\frac{1}{2}° \times \frac{1}{2}°$ version of the model; the computation was continued for another 100 yr. Similarly, the $\frac{1}{4}° \times \frac{1}{4}°$ model was then initialized with the $\frac{1}{2}° \times \frac{1}{2}°$ solution and integrated for another 120 yr. Finally, the $\frac{1}{8}° \times \frac{1}{8}°$ model was integrated for 126 yr, which resulted in a quasi-equilibrium state with a drift in volume-averaged temperature of $0.26°$ for 100 yr, as estimated from the total (surface and lateral) heat flux.

The simulated stratification is in good overall agreement with the data from the *World Ocean Atlas* (Boyer et al. 2005). The pycnocline is, however, somewhat shallower than the observed one. We attribute this bias to the limited meridional extent of our domain, as the lateral sponge boundary conditions cannot fully represent the tropics and the Southern Hemisphere in the model [see Booth and Kamenkovich (2008) for a detailed discussion of similar biases in the 10-level version of this model]. This negative bias in the pycnocline depth could be alleviated by an unrealistically high vertical diffusivity, but at the expense of unrealistically strong diapycnal mixing and upwelling at mid- and low latitudes. By choosing the low value of vertical diffusivity, we limit the amount of diapycnal mixing to more realistic levels.

The simulated Gulf Stream has a realistic width of approximately 100 km, and it separates from the coast at around 35°N. The path of the eastward Gulf Stream extension is unsteady and is characterized by large meanders. As a result, the time-mean eastward jet is broader and weaker than in the real ocean. In addition, part of the Gulf Stream quickly turns north again and does not turn east until it reaches 40°N. All of these problems are typical of many ocean models, even more comprehensive ones than ours (e.g., Nakamura and Chao 2000). In contrast, the subpolar gyre return flow, the Labrador Current, is concentrated and coherent. Consistent with the shallow pycnocline (e.g., Gnanadesikan 1999), the meridional overturning circulation is too shallow and weak, with a maximum transport of only 10 Sv. With the exception of the topmost 200 m, the simulated time-mean flow is dominated by zonal jets, which are the subject of this study.

3. Zonal jets: Velocity, buoyancy, and vorticity structure

Well-pronounced zonal jets, with maximum speeds of several centimeters per second, are seen in the time-mean zonal velocities at all depth levels (see Fig. 1a). The jet structure is clearly visible only in the time-mean velocities. Hence we describe them as "latent" jets.[2] The instantaneous zonal velocity field in the interior of the domain is dominated by vigorous transient mesoscale eddies (Fig. 1b), which obscure the underlying jet structure in the zonal velocity, particularly in the subtropical gyre. Time averaging over a period of at least several months is required in order to reveal the jets [see also Maximenko et al. (2005) for a similar property observed in satellite data].

To quantify this "latency" of the jets, we calculated a ratio between time-mean zonal velocity and standard deviations in zonal velocity anomalies. The resulting values (not shown) vary with latitude, reaching maximum values of 0.5–1.0 in the eastward jets of the subpolar gyre. In the subtropical gyre, the values are less than 0.1 in the northern half of the gyre and less than 0.5 in the southern part. Overall, the eddies are at least as strong as the jets throughout the domain, and even dominate instantaneous velocities in most of the subtropical gyre.

Based on these features, it may be more appropriate to describe the zonal jets as a tendency of the flow to develop zonal velocity anomalies of the same sign at certain latitudes. This latent nature of the oceanic jets sets them apart from *manifest* atmospheric multiple zonal jets, which are substantially stronger than the surrounding eddies. For example, on such giant gas planets as Jupiter, the manifest jets are clearly visible as stripes of slightly different colors that have been observed for centuries (e.g., Galperin et al. 2004). In the oceans, the described latency of the zonal jets makes them qualitatively different from such intense and persistent oceanic currents as the Gulf Stream.

The meridional width of the jets is substantially longer than the Rossby deformation radius of 30–50 km. As discussed in the introduction, the eddies with the meridional scale comparable to the jet width are expected to play an important role in jet dynamics. It is not surprising, therefore, that we begin to observe the jets in simulations with intermediate resolution, such as the $\frac{1}{3}° \times \frac{1}{3}°$ simulation by Nakano and Hasumi (2005) and our own $\frac{1}{4}° \times \frac{1}{4}°$ runs (not shown). The jets, however,

---

[2] A reviewer has suggested the term "pseudo jets," however, we feel the jets are merely masked by the eddy field but are not artifacts of the averaging.
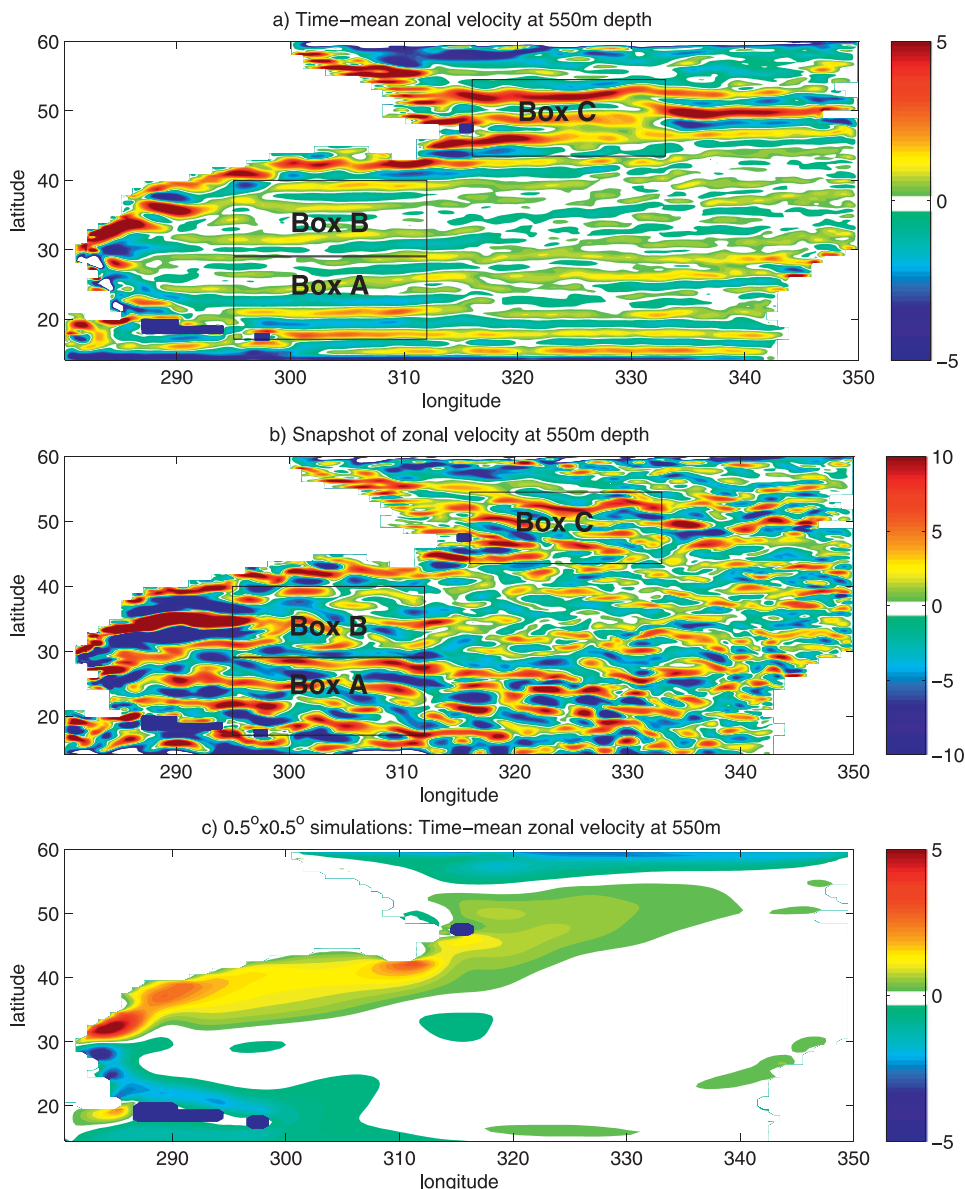
FIG. 1. Zonal velocities at the depth of 550 m in eddy-resolving simulations; the units are 10^{-2} m s^{-1}: (a) 9-yr-mean values and (b) a snapshot. Note the different color range between (a) and (b). Three box regions, A, B and C, are shown by the black lines. (c) Zonal velocity at 550 m in an ''eddy-free'' $\frac{1}{2}° \times \frac{1}{2}°$ simulation.

are not reproduced by our numerical simulations with the spatial resolution of $\frac{1}{2}° \times \frac{1}{2}°$ (Fig. 1c), which employ the Laplacian viscosity of 2.5×10^4 m^2 s^{-1}. Such strong dissipation is necessary, in particular, to make the viscous (Munk) boundary layer resolvable (Griffies and Hallberg 2000), but suppresses eddies and jets. Crudely resolved jets become visible only when the viscosity is substantially reduced. Our additional $\frac{1}{2}° \times \frac{1}{2}°$ run with the biharmonic viscosity of 10^{11} m^4 s^{-1} does exhibit jets (not shown), but the viscous boundary layer (22 km

wide) is not resolved, which casts doubt on the overall accuracy of the results (Griffies and Hallberg 2000).

a. Velocity structure

The jets are present at all latitudes and depths (Fig. 1a), although their properties vary with geographical location. In the latitude band between approximately 25° and 35°N, the meridional position of the jet axes drifts southward with typical speeds of 0.002–0.0035 m s^{-1}, resulting in the weak 9-yr mean. In the rest of the

domain, we do not observe any significant variations in the position of the jets over the course of 30 yr. The strongest jets are found in the subpolar gyre, where the maximum velocity exceeds 0.1 m s^{-1}, and in the subtropical gyre south of 25°N, where the velocities reach 0.05 m s^{-1}.

Properties of the jets, as will be shown in the following analysis, depend on the direction and structure of the background gyre flow, which is defined here as the low-pass spatially filtered, time-mean flow.[3] For example, the high intensity of the subpolar jets and eddies is consistent with a stronger, more supercritical vertical shear in the background flow in this region (see also LaCasce and Pedlosky 2004). It is, therefore, convenient to consider separately three regions with predominantly zonal background flow: the southern half of the subtropical gyre with the westward background flow (box A in Fig. 1), the northern half of the subtropical gyre with the eastward background flow (box B), and the southern part of the subpolar gyre with the eastward background flow (box C). The background meridional velocity is predominantly southward in boxes A and B (subtropical gyre) and northward in box C (subpolar gyre).

Within the limits of the quasigeostrophic theory, the vertical structure of the flow can be described by a set of the orthogonal vertical modes, $\varphi_n(z)$. We apply quasigeostrophic approximation *locally* within the interior of the gyres and find these modes as eigenvectors, $\varphi_n(z)$, of the eigenvalue problem (Pedlosky 1987):

$$\frac{\partial}{\partial z}\left(\frac{f^2}{N^2}\frac{\partial \phi_n}{\partial z}\right) = -\lambda_n \phi_n, \quad (1)$$

where z is the vertical coordinate and N is the Brünt–Väisälä frequency. Note that each mode $\varphi_n(z)$ is also a slowly varying function in x and y. The three first baroclinic modes are shown as functions of depth in Figs. 2a–c; note much weaker and more uniform stratification in the subpolar gyre. These local vertical modes allow us to conveniently describe the three-dimensional velocity by a small number of two-dimensional variables—the local projections of the velocity on the vertical modes. In particular, the projection of zonal velocity u on the nth vertical mode is defined as

$$U_n(x, y) = \langle u(x, y, z)\phi_n(z; x, y)\rangle[\langle \phi_n(z; x, y)^2\rangle]^{-1}, \quad (2)$$

where the angle brackets $\langle \rangle$ hereafter stands for the vertical average. The first three projections, $U_{1,2,3}$,

zonally averaged within boxes A, B, and C are shown in Fig. 2d together with the depth-averaged, or "barotropic," component $U_0(x, y) = \langle u \rangle$.

The vertical structure of the jets differs between the "box" regions. In the southern part of the subtropical gyre (box A), the vertical structure of the zonal velocity is dominated by the barotropic and first two baroclinic modes. As suggested by these results, the geostrophic motions in this region can be successfully approximated by the three-layer QG model, which is consistent with the prediction by an idealized model in BKPa and BKPb. The multiple zonal jets manifest themselves as the alternating maxima–minima in the zonal means of $U_{0,1,2,3}(x, y)$. The locations of maxima–minima in the barotropic (U_0) and baroclinic ($U_{1,2,3}$) components do not coincide, indicating that the meridional positions of the jet axis vary with depth. This conclusion is not consistent with BKPb, suggesting that the inhomogeneity of the background flow has an important role. At the latitudes between 33° and 37°N (box B), all three vertical modes are important; the time-mean jets are, however, relatively weak in this region (Fig. 1a). The subpolar gyre (box C) is dominated by the barotropic and first baroclinic modes; hence the geostrophic dynamics can be approximated by the two-layer QG model, consistent with BKPa and BKPb. The positions of the jet axes do not vary with depth in box C; the axes of the barotropic and baroclinic jets—maxima–minima in U_0 and U_1—are located at the same latitudes. Note that the barotropic component is particularly large in the subpolar gyre, where the stratification is nearly uniform (Figs. 2a–c). This is consistent with Smith and Vallis (2001, 2002), who predicted that the energy in uniformly stratified turbulent flows is expected to go into the barotropic mode.

With the velocities of several centimeters per second, the jets dominate the zonal velocity field at the depths below 200 m. The background flow, defined through the low-pass filtering described above, is noticeably weaker than the jets (high-pass-filtered data) in all three leading components, $U_{0,1,2}$. The ratio between the strengths of the jets (at the jet axes) and of the background velocities is greater than 5 for all jets, and larger than 10 for most of the jets. The jets clearly dominated the zonal velocities in the bulk of the ocean. Above 150–200 m, the jet velocities are comparable to those of the background flow, which is explained by strong near-surface large-scale currents.

The meridional scale of the jets is estimated for each of the components $U_{0,1,2}$ within each of the box regions. We project zonally averaged $U_{0,1,2}$ on the Fourier modes in the meridional direction, and calculate the corresponding power spectra. The results demonstrate a

---

[3] The filtering is achieved by the triple smoothing in the meridional direction with the 5° running mean filter.
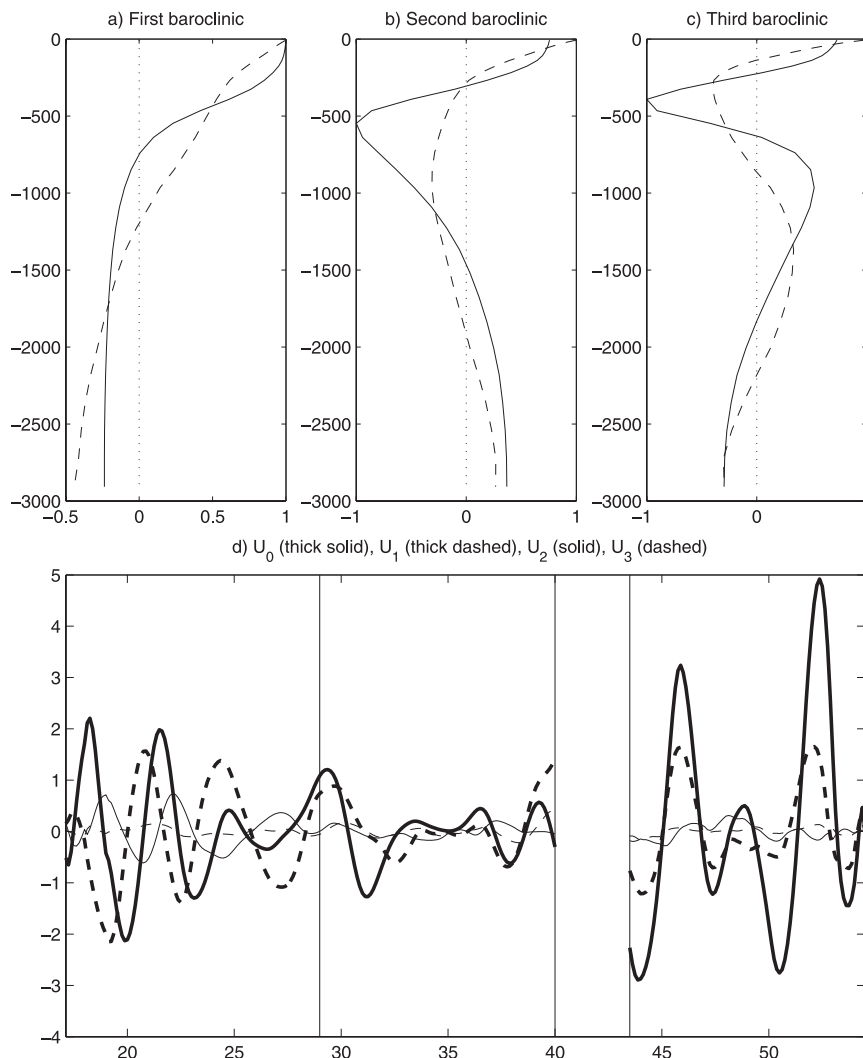
FIG. 2. Stratification and vertical structure of the time-mean zonal velocities. (top) First three local baroclinic modes inside the subtropical (30°N, solid) and subpolar (50°N, dashed) gyres. (bottom) Projections of zonal velocities on vertical modes, U_0 (heavy solid), U_1 (heavy dashed), U_2 (thin solid), and U_3 (thin dashed). Values are zonally averaged within regions A, B, and C. The latitudinal boundaries of these regions are marked with vertical lines.

well-pronounced peak at the wavelength of 3.2°–4.0° for all boxes, suggesting that the jets have a width of 1.6°–2.0°. We also estimate the Rhines scale (Rhines 1975), $R_L = (2U/\beta)^{1/2}$, where U is the square root of barotropic eddy kinetic energy (Panetta 1993) and β is the planetary vorticity gradient. The values (not shown) are nearly uniform in the entire subtropical gyre, but exhibit an increase in the southern half of box C and the subsequent northward decrease. The proper validation of the Rhines scaling requires examination of the jet properties for various values of parameters, such as β, which is difficult to achieve in this study. Such an analysis is performed in an idealized channel model of

BKPb, who report significant disagreement between the jet width and the Rhines scaling.

Several important features distinguish the jets in this study from the jets in a zonally periodic domain. First, here we do not observe asymmetry between the eastward and westward jets that is seen in the zonally periodic domains (Panetta 1993; BKPa; BKPb). Second, the jet amplitudes increase westward in most of the subtropical gyre. This is consistent with the enhancement of eddy amplitudes as the eddies propagate westward, as discussed in LaCasce and Pedlosky (2004), and is also observed in the *closed-basin* solutions in BKPb. Finally, the jets within the northern subtropical gyre

drift southward with typical speeds of 0.002–0.0035 m s^{-1}. Richards et al. (2006) report similar results for the midlatitude North Pacific and BKPb describe an analogous drift of the jets in the westward background flow in a closed basin. The meridional migration of the jets results in their weakened signature in the time-mean velocity fields.

b. Momentum and relative vorticity

The equations for x- and y-momentum components are written as

$$\frac{\partial u}{\partial t} + \mathbf{u} \cdot \nabla u - fv = -\frac{1}{\rho}\frac{\partial P}{\partial x} + F_x,$$
$$\frac{\partial v}{\partial t} + \mathbf{u} \cdot \nabla v + fu = -\frac{1}{\rho}\frac{\partial P}{\partial y} + F_y, \qquad (3)$$

where f is the Coriolis parameter, P is pressure, ρ is density, and (F_x and F_y) are the viscous terms for u and v velocity.[4] Equations (3) are dominated by the geostrophic balance, and the Coriolis terms $-fv$ and fu exceed nonlinear advection terms by two orders of magnitude. To establish the role of eddies in driving zonal jets, we take the curl of the horizontal momentum equations. This procedure eliminates the linear geostrophic terms and yields the equation for the vertical component of the relative vorticity, $\varsigma = (\partial v / \partial x) - (\partial u / \partial y)$ (e.g., Vallis 2006):

$$\frac{\partial \zeta}{\partial t} = -\mathbf{u} \cdot \nabla \zeta - \beta v + f\frac{\partial w}{\partial z} + \Phi_{\text{DIST}} + \Phi_{\text{BCL}} + \Phi_{\text{FRIC}}, \qquad (4)$$

where the first three terms on the right-hand side of (3) are, from left to right, the advection of the relative vorticity, advection of the planetary vorticity, and the linear stretching term. Note, however, that the third term is influenced by the nonlinear production of vertical velocity by eddies. In the QG dynamics, this term is closely related to the form stress forcing in the PV equation, through the buoyancy equation (Pedlosky 1987). The remaining terms are the nonlinear stretching term,

$$\Phi_{\text{DIST}} = \left(\frac{\partial u}{\partial z}\frac{\partial w}{\partial y} - \frac{\partial v}{\partial z}\frac{\partial w}{\partial y} + \zeta\frac{\partial w}{\partial z} \right),$$

the vertical component of the baroclinic vector,

$$\Phi_{\text{BCL}} = \frac{1}{\rho^2}\left(\frac{\partial P}{\partial y}\frac{\partial \rho}{\partial x} - \frac{\partial P}{\partial x}\frac{\partial \rho}{\partial y} \right),$$

---

[4] For convenience, all equations in this manuscript are written in the local, Cartesian coordinate frame. Analysis of the GCM equations of motion is carried in spherical coordinates.

and the dissipative term,

$$\Phi_{\text{FRIC}} = \left(\frac{\partial F_y}{\partial x} - \frac{\partial F_x}{\partial y} \right).$$

We find that the eddies directly affect time-mean relative vorticity mainly through the nonlinear advection of relative vorticity, since the nonlinear terms Φ_{DIST} and Φ_{BCL} are found to be small. The smallness of the latter two terms makes an analogy with the QG dynamics meaningful and allows us to relate the findings in this study to those in a QG model in BKPa and BKPb. This connection is, however, not always straightforward, mainly because of the difference in the background flow—generally weak nonzonal gyre flow in this model versus strong purely zonal current in BKPa and BKPb—and is likely to cause disagreements in results.

Following the traditional approach, we isolate the effects of eddies by splitting velocities into the time-mean part $\overline{\mathbf{u}}$ and the deviations from such mean, or "eddy" velocities $\mathbf{u}'$, and analyzing the time mean of (3). The time-mean, nonlinear advection term then splits into the eddy–eddy and mean–mean parts:

$$-\overline{\mathbf{u} \cdot \nabla \zeta} = -\overline{\mathbf{u}' \cdot \nabla \zeta'} - \overline{\mathbf{u}} \cdot \nabla\overline{\zeta}. \qquad (5)$$

The first term on the right-hand side of (5), the eddy advection of vorticity anomalies with a negative sign, is referred to as the "Reynolds stress eddy forcing." The time-mean, zonally averaged relative vorticity has well-pronounced banded structure (Fig. 3a) associated with the zonal jets. Our main objective here is to determine the role of eddy forcing in sustaining this structure. Since the horizontal structure of the barotropic and baroclinic components of the velocity varies across the domain (see the previous section), we can expect barotropic and baroclinic eddies to play different roles in the dynamics of the jets. To establish a link between barotropic and baroclinic dynamics in the system, we analyze the barotropic and baroclinic vorticity separately. Note, however, that the barotropic eddies are likely to be products of baroclinic instability themselves, and the baroclinic and barotropic dynamics are coupled.

We begin with the analysis of the barotropic vorticity. In Fig. 3a, we plot the zonally and depth-averaged eddy–eddy term [first term on the right-hand side of Eq. (4)] and all terms that depend on the time-mean fields only, including the mean–mean advection term [second term in Eq. (5)], advection of the planetary vorticity, and the wind stress term $\nabla \times \boldsymbol{\tau}$. Note that the presence of the mean advection term, $-\overline{\mathbf{u}} \cdot \nabla\overline{\zeta} - \beta\overline{v}$, complicates the analysis. In a zonally periodic domain (e.g., Panetta 1993; BKPa; BKPb), the mean advection terms are absent from the zonal-mean vorticity balance,
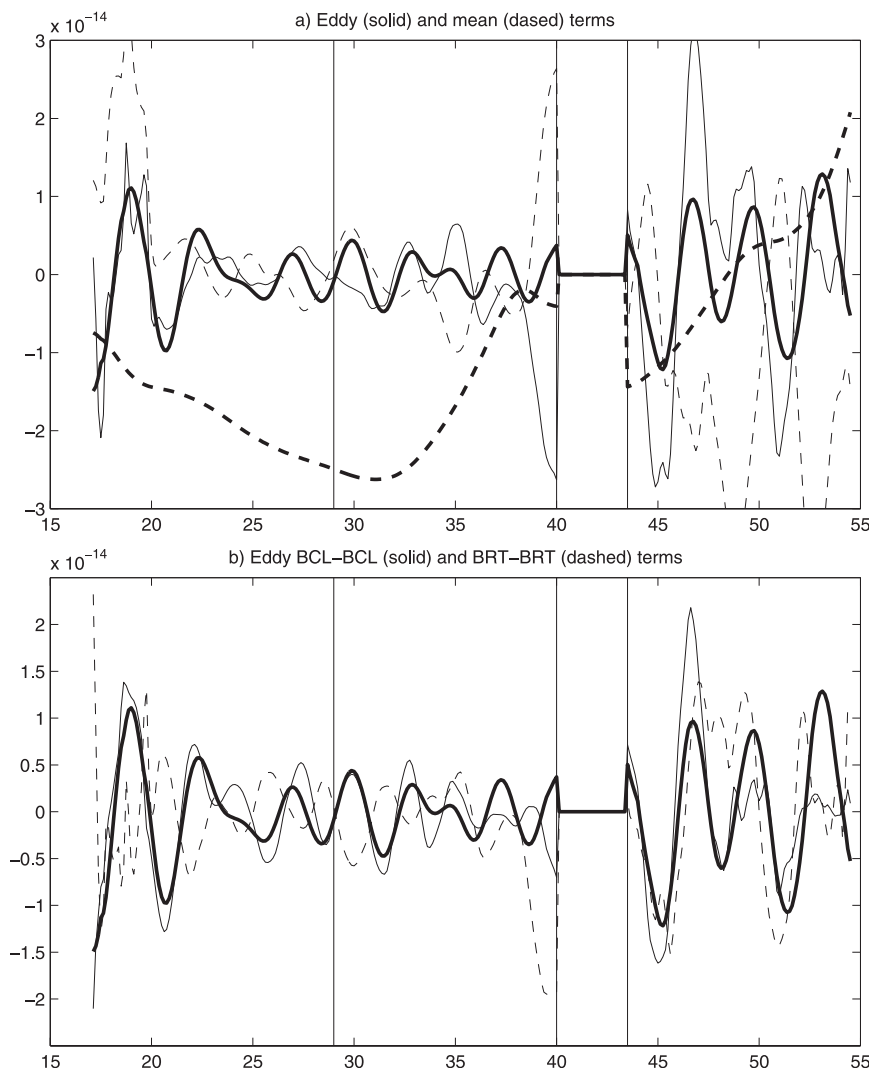
FIG. 3. Role of eddies in supporting barotropic jets. (a) Vertically averaged eddy (thin solid) and mean (dashed) advection terms in the equation for the relative vorticity; see the text and Eq. (4). Also shown is the wind stress curl (thick dashed). The terms are zonally averaged within the regions A, B, and C; the latitudinal boundaries of the regions are marked with vertical lines. (b) Zonal-mean BRT–BRT (dashed) and BCL–BCL (thin solid) eddy terms; see the text. The zonal-mean barotropic relative vorticity, scaled to be comparable in magnitude to the advective terms, is shown by the heavy solid line in (a) and (b).

and the net eddy forcing always supports the jets and balances dissipation. In our case, the dissipation of the jets is balanced by a sum of the mean advection terms and Reynolds stress eddy forcing, and the interpretation of the role of eddy forcing is less straightforward. As discussed in the introduction, our approach is to interpret the spatial correlation between particular eddy forcing and the vorticity anomalies associated with the jets. If such correlation is positive, we conclude that the eddy forcing supports the jets.

The maxima–minima in the eddy–eddy advection term (thin solid line) and the vorticity (heavy solid line) tend

to be in phase within boxes A and C, with the corresponding correlation coefficients 0.83 and 0.70, respectively. The eddy forcing maintains the jets. The action of this eddy forcing is compensated by the time-mean terms (dashed line) and dissipation (not shown). In contrast, the correlation between the barotropic relative vorticity and eddy forcing is weak in box B, and the correlation coefficient is close to zero. Also plotted in Fig. 3a is the zonal-mean wind stress curl (the thick dashed line), which does not exhibit variations on the spatial scales of the jets and therefore cannot directly induce the jetlike structure.

To shed light on the relative importance of the barotropic and baroclinic dynamics, we separate the eddy velocities, $\mathbf{u}'$, into the depth-averaged (barotropic) component, $\langle \mathbf{u}' \rangle$, and the residual (baroclinic) component, $\mathbf{u}'* = \mathbf{u}' - \langle \mathbf{u}' \rangle$. The vertically averaged, time-mean horizontal components of the Reynolds stress forcing then each split into two components (using subscripts x, y, and z for corresponding derivatives):

$$\overline{\langle u' \zeta'_x \rangle} = \overline{\langle u'* \zeta'_x* \rangle} + \overline{\langle u' \rangle \langle \zeta'_x \rangle};$$
$$\overline{\langle v' \zeta'_y \rangle} = \overline{\langle v'* \zeta'_y* \rangle} + \overline{\langle v' \rangle \langle \zeta'_y \rangle}. \qquad (6)$$

The time-mean, vertically averaged vertical advection splits into

$$\overline{\langle w' \zeta'_z \rangle} = \overline{\langle w'* \zeta'_z* \rangle} + \overline{\langle w' \rangle \langle \zeta'_z* \rangle}. \qquad (7)$$

The first terms on the right-hand sides of (6) and (7) stand for the advection of baroclinic vorticity by baroclinic velocities ("baroclinic–baroclinic" term or "BCL–BCL"). The second terms on the right-hand side of (6) stand for the advection of the barotropic vorticity by the barotropic velocities ("barotropic–barotropic" term or "BRT–BRT"). The last term on the right-hand side of (7), the mixed barotropic–baroclinic term, is verified to be small compared to the other terms in (7). For convenience, we add it to the BCL–BCL terms in the following analysis.

The self-interactions of the baroclinic eddies maintain the barotropic jets through the Reynolds stress forcing. Zonal averages of the two Reynolds stress terms, BRT–BRT and BCL–BCL, are plotted in Fig. 3b. The maxima–minima in the BCL–BCL eddy term are in phase with the maxima–minima in the vorticity in all boxes A, B, and C; the corresponding correlation coefficients are 0.92, 0.47, and 0.73, respectively. In contrast, the BRT–BRT term is negatively correlated with the vorticity in regions A and B (correlation coefficients −0.34 and −0.23), which is interpreted as a resisting effect of barotropic eddies on the barotropic jets. This result is in contrast with findings in idealized studies in a zonal channel (e.g., BKPb), where the interactions between barotropic eddies act to sustain the jets. The BRT–BRT eddy forcing in box C acts to maintain the jets (correlation coefficient 0.48), in agreement with the results in BKPb.

We next consider the baroclinic vorticity balance, and plot the projections of the Reynolds stress term and the sum of all terms depending on time-mean velocities on the first vertical mode φ_1 (Fig. 4a). In contrast to the barotropic balance, the baroclinic Reynolds stress forcing acts to weaken most of the baroclinic jets in the subtropical gyre (boxes A and B); the corresponding correlation coefficients are, however, rather weak: near 0 and −0.29. The situation is the opposite in the subpolar gyre, box C. In this region, the baroclinic jets are supported by eddies, as suggested by the strong positive correlation (correlation coefficient 0.65) between the Reynolds stress forcing and baroclinic vorticity; this result is consistent with BKPb.

To get further insight into the interaction between barotropic and baroclinic modes, we once again separate the eddy velocities into the barotropic component, $\langle \mathbf{u}' \rangle$, and baroclinic component, $\mathbf{u}'*$; the baroclinic advection term then splits into four components:

$$(\overline{\mathbf{u}' \cdot \nabla \zeta'})* = \overline{\mathbf{u}'* \cdot \langle \nabla \zeta' \rangle} + \overline{\langle \mathbf{u}' \rangle \cdot \nabla \zeta'*}$$
$$- \overline{\langle w' \rangle \langle \zeta'_z* \rangle} + (\overline{\mathbf{u}'* \cdot \nabla \zeta'*})*. \qquad (8)$$

The first three terms on the right-hand side of (8) represent mixed barotropic–baroclinic interactions and the last term represents baroclinic–baroclinic interactions (with the vertical average removed). We next project BRT–BCL and BCL–BCL eddy forcings on the first vertical mode and plot these projections, zonally averaged, in Fig. 4b. The BRT–BCL eddy forcing has a resisting effect on the baroclinic jets in box B (correlation coefficient −0.37) and the northern part of box A, which is consistent with BKPb. At some locations in the subtropical gyre, this effect is counteracted by the BCL–BCL eddy forcing, but the overall role of the BCL–BCL forcing is hard to establish and the corresponding correlation coefficients are close to zero. What we observe here is the transfer of vorticity away from the baroclinic jets due to the interactions between barotropic and baroclinic eddies. In box C, both the BRT–BCL and BCL–BCL eddy forcings accelerate the jets, which is manifested in the positive spatial correlation between the eddy forcing and baroclinic vorticity; the corresponding correlation coefficients are 0.58 and 0.80. Once again, the results in the subpolar gyre are consistent with findings in BKPb.

c. Density

We next consider the role of the mean and eddy advection in maintaining the distribution of density. The equation for the potential density $\sigma(T, S)$ is obtained by multiplying the equations for temperature and salinity by $\partial \sigma(T, S)/\partial T$ and $\partial \sigma(T, S)/\partial S$, and adding the results together. We analyze the effects of eddies within the framework of the Transformed Eulerian Mean (TEM;
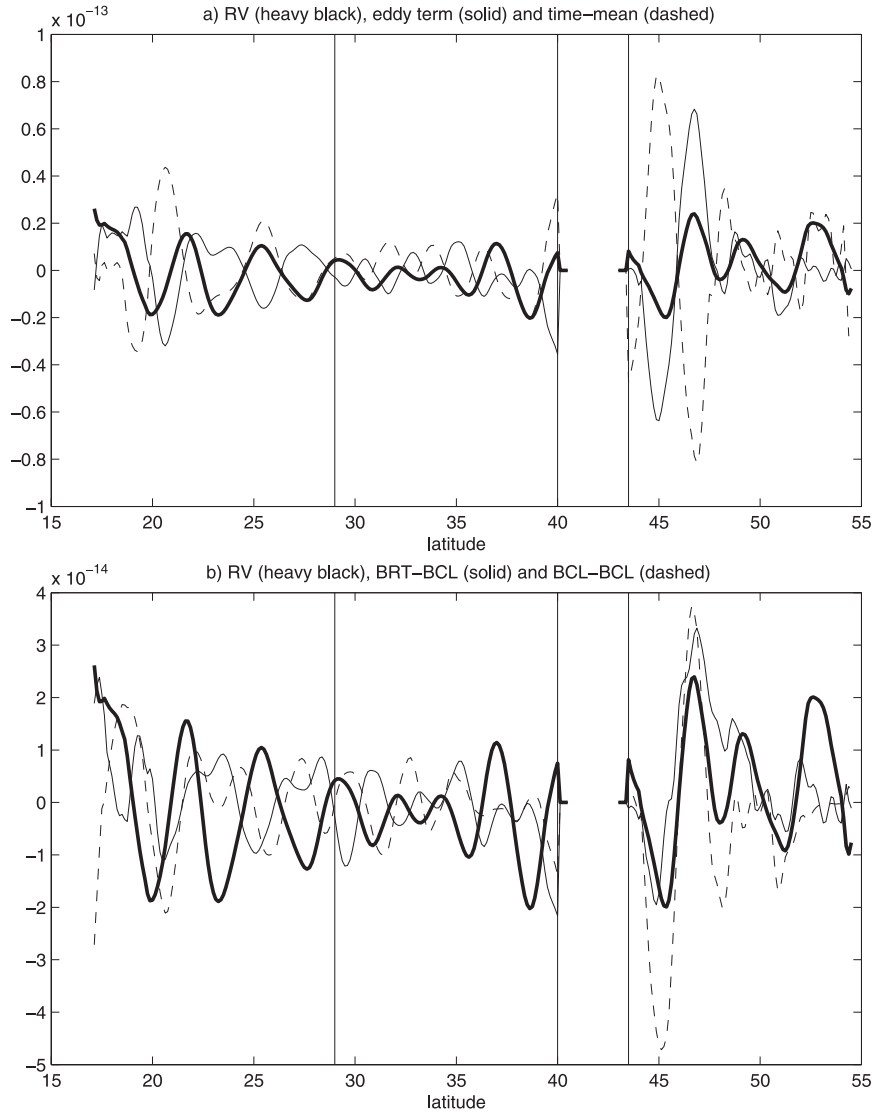
FIG. 4. Role of eddies in supporting baroclinic jets. (a) Projection of the baroclinic terms in the equation for the relative vorticity (3) on the first vertical mode $\varphi_1(z)$. The eddy (thin solid) and mean (dashed) advection terms are zonally averaged within the regions A, B, and C; the latitudinal boundaries of the regions are marked with vertical lines. (b) Zonal-mean BRT–BCL (solid) and BCL–BCL (dashed) eddy forcings; see the text. The zonal-mean baroclinic relative vorticity, scaled to be comparable in magnitude to the advective terms, is shown by the heavy solid line in (a) and (b).

Andrews and McIntyre 1976), where the eddy density fluxes are expressed in terms of the eddy-induced velocities (u_e, v_e, and w_e). Taking the time average and ignoring the time evolution term, we can write the equation for density in the following convenient form:

$$(\overline{\mathbf{u}} + \mathbf{u}_e) \cdot \nabla \overline{\sigma} = -\frac{\partial G}{\partial z} + \overline{\Phi}_{\mathrm{DIFF}}, \qquad (9)$$

where the eddy-induced velocities are defined through the eddy fluxes and the mean stratification:

$$u_e = -\frac{\partial}{\partial z}\left(\frac{\overline{u'\sigma'}}{\partial \overline{\sigma}/\partial z}\right), \quad v_e = -\frac{\partial}{\partial z}\left(\frac{\overline{v'\sigma'}}{\partial \overline{\sigma}/\partial z}\right),$$

$$w_e = \frac{\partial}{\partial x}\left(\frac{\overline{u'\sigma'}}{\partial \overline{\sigma}/\partial z}\right) + \frac{\partial}{\partial y}\left(\frac{\overline{v'\sigma'}}{\partial \overline{\sigma}/\partial z}\right). \qquad (10)$$

The terms on the left-hand side of (9) stand for the total (mean plus eddy) convergence of density fluxes on time-mean isopycnal surfaces. The function $G(x, y, z)$ is proportional to the flux of density in the direction normal to the time-mean isopycnal surfaces:
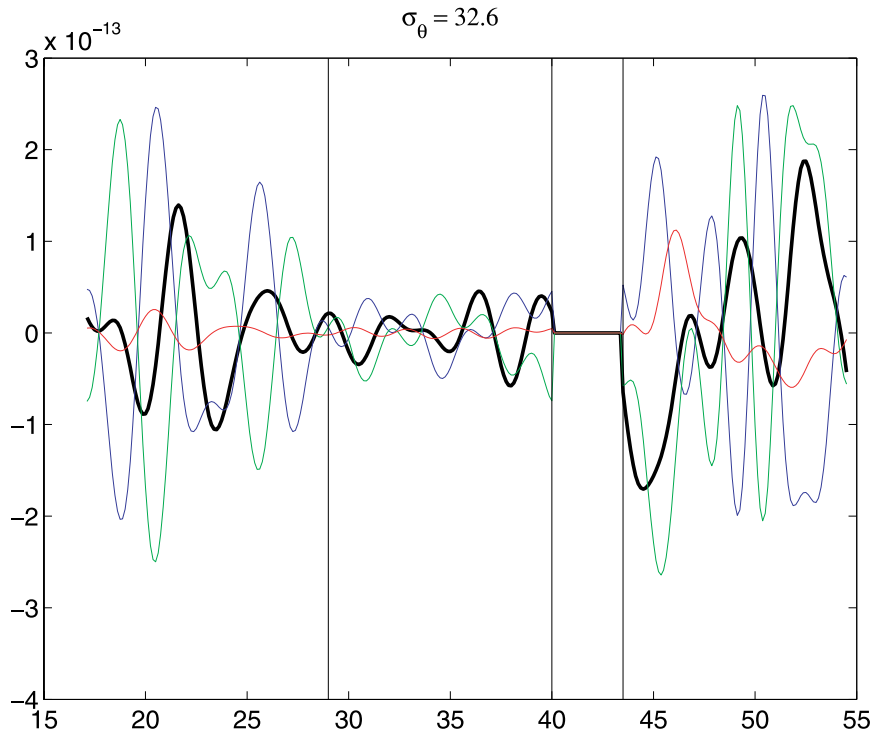
FIG. 5. Role of eddies in the density balance. Density evolution terms in Eq. (8) are plotted on isopycnal $\sigma_\theta = 32.6$, zonally averaged within regions A, B, and C. The terms shown are the along-isopycnal, eddy-induced advection (blue), mean advection (green), and cross-isopycnal eddy advection (red) terms. The isopycnal height anomaly z_σ, scaled to be comparable to the density evolution terms, is shown by the heavy solid line.

$$G = \frac{\overline{\mathbf{u}'\sigma'} \cdot \nabla\overline{\sigma}}{\partial\overline{\sigma}/\partial z}. \tag{11}$$

Note that the function $G(x, y, z)$ can be nonzero even for the purely adiabatic (density conserving) motions, since $G(x, y, z)$ is proportional to the eddy flux across the *time-mean* isopycnals. It is, therefore, important to understand the distinction of this term from the time-mean diapycnal flux, which is zero if the motion is adiabatic. The remaining terms on the right-hand side of (9) are diabatic diffusive terms, and are nonlinear functions of temperature, salinity, and density.

We next consider the isopycnal height anomaly, Z_a, defined as the difference between the actual isopycnal height $Z(\sigma)$ (distance from the bottom) and its value smoothed with the 5° running-mean filter, so $Z_a = Z - \tilde{Z}$, where the tilda stands for the spatial smoothing. The isopycnal height anomalies exhibit banded structure, seen as a series of alternating maxima–minima in their zonal average. The values are reported in Fig. 5 on the isopycnal $\sigma_\theta = 32.6$, whose depth varies between approximately 1000 m in the subtropical gyre to 500 m in the subpolar gyre. Since the meridional gradient of the isopycnal height is tied to the vertical shear in zonal

velocity through the thermal wind balance, this banded structure is a manifestation of the geostrophic jets. Figure 5 also shows zonally averaged density evolution terms in (9) on $\sigma_\theta = 32.6$: the mean advection, $-\overline{\mathbf{u}} \cdot \nabla\overline{\sigma}$, eddy-induced advection (eddy forcing), $-\overline{\mathbf{u}}_e \cdot \nabla\overline{\sigma}$, and the cross-isopycnal term $\partial G/\partial z$. For the convenience of the interpretation of the spatial structure of eddy forcing, we filter out variations on spatial scales shorter than 1° and longer than 3° using a Fourier transform in the meridional direction.

The two advection terms, the mean and eddy induced, dominate the density balance. The eddy-induced advection term $-\overline{\mathbf{u}}_e \cdot \nabla\overline{\sigma}$ is "in phase" with the isopycnal height anomaly Z_a for several jets in the subtropical gyre. Since the convergence of density (mass) flux acts to shoal isopycnals, this positive correlation implies that the eddy-induced term acts to maintain the "banded" structure in the isopycnal height anomaly. This property is in apparent disagreement with the common assumption that mesoscale eddies act to smooth isopycnals, thus removing the available potential energy from the flow. The finding is, however, in general agreement with the role of baroclinic eddy forcing, the form stress forcing, in the westward background flow in BKPb. On
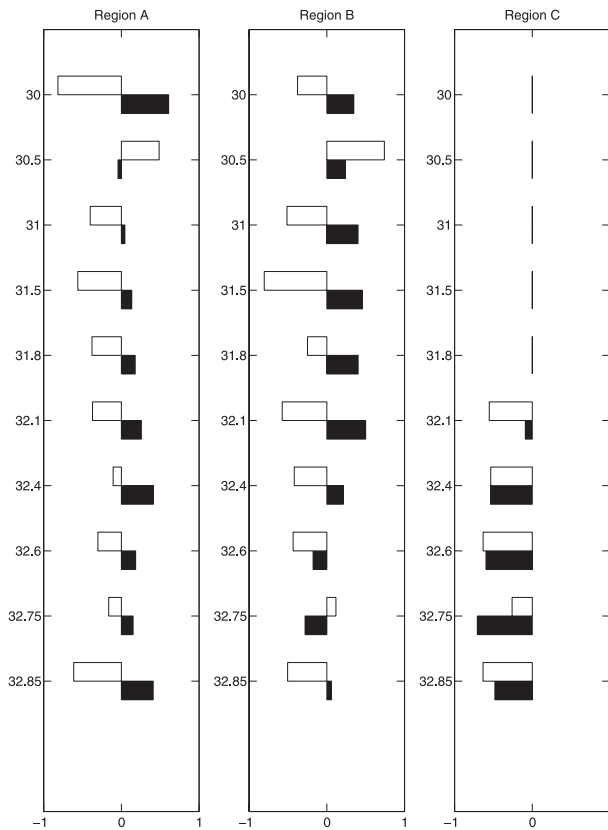
FIG. 6. Role of eddies in the density balance. Spatial correlation between zonally averaged isopycnal height anomalies and eddy density evolution terms: along-isopycnal, eddy-induced advection term (black) and cross-isopycnal eddy advection (white). The correlation is computed separately in each of the three regions: (left) region A, (middle) region B, and (right) region C on ten isopycnal surfaces. Positive correlation implies that a corresponding density evolution term acts to sustain the banded structure in the isopycnal height (see text).

the other hand, the eddy forcing acts to destroy the banded structure in the isopycnals for other jets, most notably the jets in box C, in accord with the eastbound flow in BKPb. Figure 6 presents the spatial correlation between the density terms in (9) and Z_a for ten isopycnal surfaces. The overall spatial correlation between the eddy forcing and isopycnal height anomaly Z_a in the subtropical gyre is weakly positive for most isopycnal surfaces, and is strong and negative in the subpolar gyre.

The sum of the two advective terms on the left-hand side of (9), the total TEM advection term (not shown), is partially compensated for by the cross-isopycnal eddy forcing $\partial G/\partial z$. In agreement with Henning and Vallis (2004), the magnitude of the cross-isopycnal term $\partial G/\partial z$ increases toward the surface, which can be seen by following this term northward along the isopycnal $\sigma_\theta = 32.6$ (Fig. 6); this isopycnal shoals considerably north of

45°N. The term $\partial G/\partial z$ is mostly out of phase with the isopycnal height anomaly Z_a in the subtropical gyre, thus acting to "iron out" the isopycnals. The correlation is particularly large (-0.90) for the $\sigma_\theta = 31.5$ isopycnal. The convergence of the cross-isopycnal eddy forcing resists the jets.

d. Potential vorticity

Transformation of potential vorticity, a scalar quantity, provides a useful framework for describing the three-dimensional baroclinic flow. We use here a conventional definition of the PV in oceanic flows: $q = (\nabla \times \mathbf{u} + f\mathbf{k}) \cdot \nabla\rho$. An interesting aspect of the meridional structure of the PV is the absence of a "PV staircase" (i.e., a series of alternating regions with sharp and near-zero meridional gradients). Such staircase like structures are reported to exist in some idealized studies of QG flows in zonally periodic domains (see introduction). Here, as well as in several other baroclinic studies, the PV structure resembles a PV washboard (BKPb). To illustrate this fact, we plot zonally averaged meridional PV gradients on two isopycnals, $\sigma_\theta = 31.0$ and 32.6 in Figs. 7a and 7c. In contrast to an ideal staircase, the meridional gradient is almost never zero in the domain. The same is true for all isopycnals and for the PV structure on geopotential surfaces.

The PV equation can be written as (Pedlosky 1987)

$$\left(\frac{\partial}{\partial t} + \mathbf{u} \cdot \nabla\right)q = (\nabla \times \mathbf{u} + f\mathbf{k}) \cdot \nabla\left(\frac{\partial \rho}{\partial t} + \mathbf{u} \cdot \nabla\rho\right) + \frac{\nabla\rho}{\rho} \cdot (\nabla \times \mathbf{F}), \qquad (12)$$

where $\mathbf{k}$ is the unit vector in the vertical direction. The two terms on the right-hand side of (12) represent sources–sinks of the PV: the diabatic term and the dissipative term. The diabatic term is important in flows with active diapycnal mixing, but is rarely included in the analysis of PV balances. In this study, we demonstrate its importance in the PV balance from scaling arguments (see appendix) and the analysis of the GCM results. In the top layer of the model this term is large and controlled by the buoyancy fluxes through the ocean surface. Away from the ocean surface, the term owes its existence to the diapycnal diffusion of temperature and salinity.

As we did previously, we separate velocities and density into the time-mean and eddy components. After keeping only the leading terms (see appendix), the time-mean (12) reduces to the balance between two groups of terms—terms depending on the time-mean fields (mean–mean terms) plus the dissipative term and the eddy forcing (eddy–eddy terms):
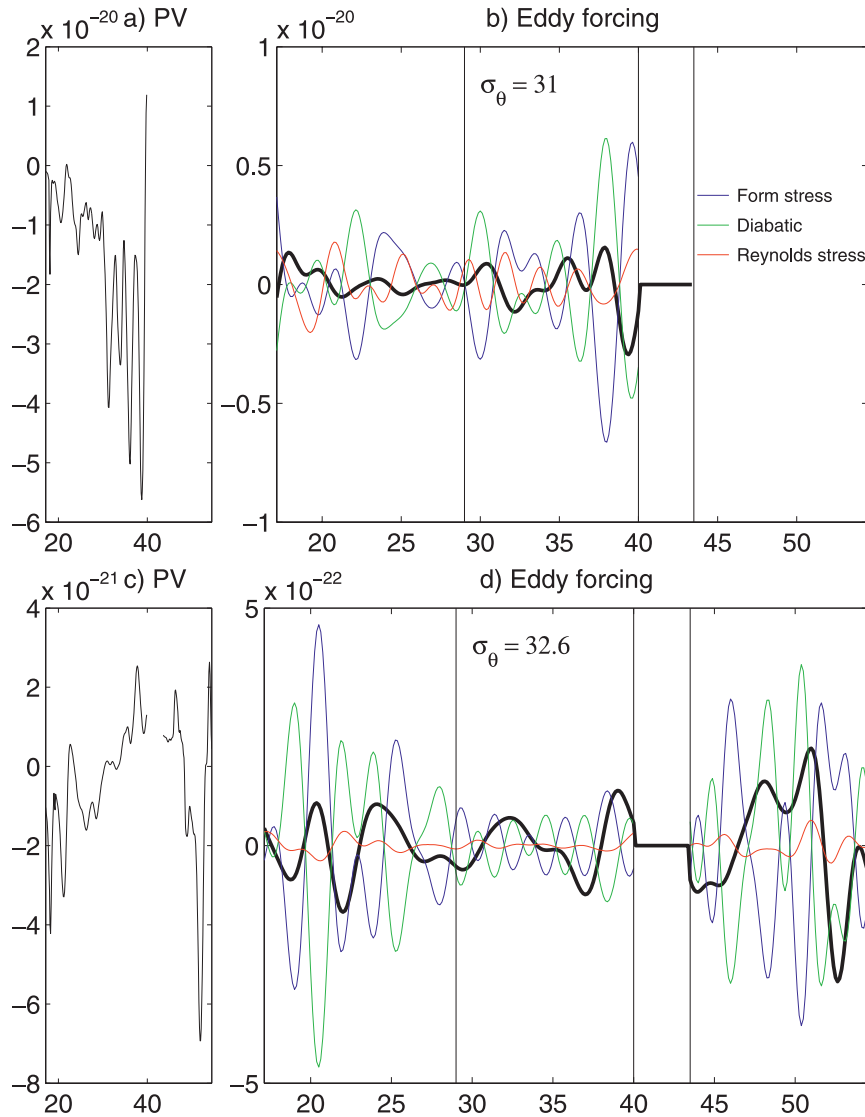
FIG. 7. PV structure and the role of eddies in sustaining it. (a) PV meridional gradients, zonally averaged within regions A, B, and C, and (b) PV evolution terms (see text). The values are given on two isopycnals, (a),(b) $\sigma_\theta = 31.0$ and (c),(d) $\sigma_\theta = 32.6$. Main forcing terms shown are the form stress forcing (blue), the diabatic forcing (green), and the Reynolds stress forcing (red). The PV anomaly, scaled to be comparable to the PV evolution terms, is shown by the heavy solid line.

$$\overline{\mathbf{u}} \cdot \nabla \left((f + \overline{\zeta}) \frac{\partial \overline{\rho}}{\partial z} \right) - f \frac{\partial}{\partial z} (\overline{\mathbf{u}} \cdot \nabla \overline{\rho}) + \overline{\frac{\nabla \rho}{\rho} \cdot (\nabla \times \mathbf{F})}$$

$$\approx -\overline{\mathbf{u}' \cdot \nabla \left(\varsigma' \frac{\partial \overline{\rho}}{\partial z} \right)} - \overline{\mathbf{u}' \cdot \nabla \left(f \frac{\partial \rho'}{\partial z} \right)} + f \frac{\partial}{\partial z} \overline{(\mathbf{u}' \cdot \nabla \rho')}.$$

$$(13)$$

The terms on the right-hand side of (13) represent PV eddy forcing terms (sources of PV due to eddy activity). The first eddy forcing term is the eddy advection of

anomalies in the relative vorticity, multiplied by the mean stratification term; we will refer to it as the "generalized Reynolds stress forcing." The second term represents eddy advection of vertical density gradient anomalies, multiplied by the planetary vorticity; we will refer to it as the "generalized form stress forcing." The third term on the right-hand side is the eddy component of the diabatic source term in (12), "diabatic eddy forcing" hereafter. This diabatic forcing is only partially balanced by the analogous mean–mean diabatic term on

the left-hand side of (13); the residual is compensated for by the diapycnal diffusion.

The zonally averaged PV anomaly, q_a, scaled to be comparable to the PV evolution terms, is plotted in Figs. 7b and 7d on $\sigma_\theta = 31.0$ and 32.6; the overall structure is very similar on all isopycnals. Similarly to the definition of isopycnal depth anomalies of the previous section, the PV anomaly is computed by subtracting the smoothed PV from the full PV ($q_a = q - \tilde{q}$) and further filtering using the Fourier transform (section 3c). The banded structure, associated with the zonal jets, is seen in the zonal-mean PV anomalies as alternating maxima and minima. The width of these "bands" varies with latitude, but the dominant meridional scale is 2°–2.5°, as estimated by the Fourier method. The PV anomaly is dominated by the term $f(y)(\partial \rho_a/\partial z)$ (where $\rho_a = \rho - \tilde{\rho}$) and the contribution of all nonlinear terms is small [see appendix and results by Nakamura and Kagimoto (2006)]. The "wavy" structure of the PV anomaly in the meridional direction is, therefore, a consequence of the similar structure in the vertical gradient of the density anomaly ρ_a. Since the meridional density gradient and zonal velocity are closely connected through the thermal wind balance, the wavy structure in density is simply an indication of the presence of the alternating baroclinic zonal jets and is not surprising.

Zonal means of all three eddy forcing terms in (13) are plotted in Figs. 7b and 7d on two isopycnal surfaces: a shallow $\sigma_\theta = 31.0$ (depths of 200–300 m) and an intermediate $\sigma_\theta = 32.6$ (depths of 500–1000 m). The form stress and diabatic eddy forcings are each larger than the Reynolds stress forcing and partially compensate for each other. For example, the form stress forcing is out of phase with the PV itself in box B at $\sigma_\theta = 31.0$ and in box C at $\sigma_\theta = 32.6$. This eddy forcing acts to destroy the banded structure in PV; the diabatic forcing term, in contrast, acts to sustain the PV washboard. The spatial correlations between q_a and eddy forcing terms on 10 isopycnals are reported in Fig. 8. The form stress forcing is out of phase with the PV anomalies on the isopycnals $\sigma_\theta < 32.6$ in the subtropical gyre, with the strongest negative correlation in box B and most of the subpolar gyre (box C). In contrast, the diapycnal eddy forcing is always compensating for the form stress forcing and therefore acts to sustain the PV washboard on most isopycnals. The correlation between both eddy forcings and PV anomalies is, however, very weak on some isopycnals, such as $\sigma_\theta = 31, 31.5, 31.8$ in box A; $\sigma_\theta = 30.5, 32.6, 32.75$ in box B; and $\sigma_\theta = 32.75$ in box C. The main resisting effect of the form stress forcing on jets is in accord with a resisting effect of the eddy forcing on baroclinic relative vorticity anomalies (see section 3b).
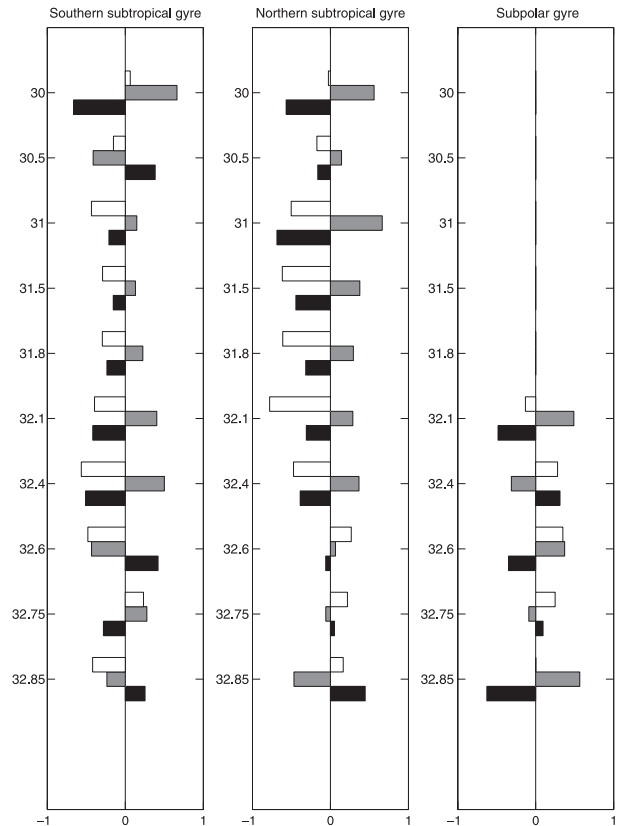

FIG. 8. Role of eddies in the PV balance. Spatial correlation between a zonal PV anomaly and eddy forcings (see text): the form stress (black), diabatic (gray), and Reynolds stress (white). The correlation is computed separately in each of the three regions: (left) region A, (middle) region B, and (right) region C on ten isopycnal surfaces. Positive correlation implies that a corresponding PV evolution term acts to sustain the banded structure in PV (see text).

Similar to the analysis of the balance for the potential density in the previous section, the diabatic eddy forcing term can be further separated into two components:

$$f\frac{\partial}{\partial z}(\overline{\mathbf{u}' \cdot \nabla \rho'}) = f\frac{\partial}{\partial z}(\mathbf{u}_e \cdot \nabla \overline{\rho}) + f\frac{\partial^2 G}{\partial z^2}. \qquad (14)$$

Analysis of the terms in (14) shows that the diabatic term is dominated by the first term on the right-hand side. This term represents a source of time-mean PV due to the vertical shear in the eddy-induced along-isopycnal advection of buoyancy. The second term, related to the cross-isopycnal flux of buoyancy, is important only in proximity to the surface, where it is positively correlated with the PV anomalies.

The Reynolds stress forcing is generally smaller in amplitude than the form stress and diabatic terms, especially in the deep ocean. The Reynolds stress forcing

is out of phase with PV anomalies in most of the subtropical gyre, above $\sigma_\theta = 32.6$. The negative correlation is particularly strong in box B (see Fig. 8b). The Reynolds stress forcing has, therefore, a resisting effect on the jets in the subtropical gyre. This result is consistent with a dissipative role of eddy fluxes in the balance for the baroclinic relative vorticity (Fig. 4a). In box C, the Reynolds stress on average acts to sustain the PV structure for the two northernmost jets (Figs. 7b,d and 8c), although the overall correlation is not very large. Similar (but much stronger) positive correlation can be found between the eddy forcing and the baroclinic relative vorticity in the subpolar gyre (Fig. 4a).

4. Summary and discussion

In this study, we describe the properties of persistent, multiple zonal jets in an eddy-resolving model of the North Atlantic. These structures are detected in satellite-based observations and are prominent features of eddying numerical simulations. In contrast, the jets are not reproduced by numerical simulations in which eddies are suppressed because of high viscosity and low spatial resolution (like the one shown in Fig. 1c). Small-scale wind anomalies cannot explain the existence of the jets, and the jets are not part of an idealized linear response to wind forcing (Nakano and Hasumi 2005). Nonlinear dynamics of eddies is thus essential for the jets, as well as for other components of basin-scale circulation (e.g., Berloff 2005b). The "eddy-free" ocean circulation, described by classical theories and simulated by low-resolution models, includes such important elements as the Sverdrup interior and western boundary currents. This and several other studies of the eddy-driven zonal jets, therefore, expand and enrich the classical picture of the eddy-free basin-scale ocean circulation.

Theories of jet formation are based on the central role of eddies in the jet dynamics (e.g., Panetta 1993; Rhines 1994; BKPa). Our findings support these conclusions and further demonstrate that eddies play a central role in supporting the jets. The fact that eddy-driven zonal jets appear in regions where the details of the eddy driving differ signifies the robustness of the mechanism of eddy driving as an explanation for the zonal jets. In particular, the barotropic components of the jets are sustained by the action of the baroclinic eddies, as demonstrated by the analysis of the relative vorticity equation. Our results thus strongly suggest that any study of the dynamics of barotropic jets needs to account for the baroclinic–baroclinic eddy forcing and its action on the jets. The role of the barotropic eddies for the barotropic jets differs between the subtropical and

subpolar gyres. The eddies act to weaken the jets in the former and to strengthen the jets in the latter region. Similarly, barotropic eddies act to resist the baroclinic jets in the subtropical gyre and support the jets in the subpolar gyre.

The potential vorticity (PV) does not exhibit the "PV staircase"—a meridional structure with alternating regions of near-zero and very sharp meridional PV gradients. Rather, we observe the "PV washboard"—the structure with alternating zonal bands of maxima and minima. These bands are associated with similar structures in the density, which are in turn consistent with the thermal wind balance in the jets. The role of eddies in supporting the corresponding "banded" structure in the isopycnal height anomalies is complex. Although in some parts of the domain the eddies act to flatten the anomalies, this is not the case everywhere. Most notably, the eddies appear to support the isopycnal height anomalies for several jets in the subtropical gyre—the action opposite to a common hypothesis that eddies tend to "iron out" isopycnals. The PV balance itself is complicated, and the nonconservative "diabatic" term plays a prominent role in the PV balance. In fact, the diabatic term is shown to support the PV washboard. These effects call for further examination. Another important eddy term, the generalized Reynolds stress forcing, supports the PV anomalies in the subpolar gyre but acts to destroy them in the subtropical gyre.

This study is the first to address the dynamics of zonal jets in the baroclinic double-gyre circulation. Previous studies focused almost exclusively on flows in zonally periodic domains, where the background flow is purely zonal, uniform, and baroclinically unstable. In this study, the spatial inhomogeneity of the background flow can potentially have important effects, which remain to be investigated. We, however, find some analogies between jets in a zonal channel (like the one in BKPa and BKPb) and in the subpolar gyre in our model. The analysis in this study, however, strongly suggests important differences between the jet dynamics in the subtropical gyre and in a channel. The difference in properties of the jets between the subtropical and subpolar regions represents one of the intriguing findings of this study. The explanation of this fact calls for further, more systematic examination.

At this point, we can only speculate about causes for the difference in jet properties between the subtropical and subpolar gyres. The stratification is more uniform in the subpolar gyre compared to the subtropical gyre, which facilitates barotropization of the eddy field according to Smith and Vallis (2001, 2002). This is consistent with a stronger barotropic component of the subpolar jets, and a stronger baroclinic component

of the subtropical jets. A systematic analysis of the importance of stratification is, however, challenging in this GCM, but is carried in idealized models of oceanic flows (BKPb). The difference in stratification is surely one of the main causes for the difference in jet dynamics between the two regions. Other factors can also be important in this GCM study. Smith and Vallis (2002) consider a horizontally uniform background state with supercritical vertical shear, whereas the background flow in our model not only has strong horizontal shear, but also exhibits different stability properties between the subtropical and subpolar regions. The vertical and horizontal shear in the current is stronger and the Rossby deformation radius is shorter in the subpolar gyre compare to the subtropical gyre. The resulting background flow is thus more baroclinically unstable, as confirmed by our analysis of the Phillips model for baroclinic instability, not described in this study. This is likely to lead to a more vigorous eddy field compared to that in the subtropical gyre.

Several remaining questions will be the subject of future studies. First, the effects of topography can be substantial and deserve careful examination. Nakano and Hasumi (2005) demonstrate that topography impedes meridional movements of the jets, but the existence of the jets and the jet width are not controlled by topographic features. The last conclusion is also in accord with our preliminary results. In particular, our primitive equation simulations in a boxlike region without topography and coastlines exhibit jets with meridional width similar to those in this North Atlantic GCM. Second, the presence of the jets can make the zonal direction the preferred direction for Lagrangian transport, with strong asymmetry between the downstream and upstream directions. Spatial anisotropy in the Lagrangian transport, investigated in a companion paper (Kamenkovich et al. 2009, manuscript submitted to *J. Phys. Oceanogr.*), can have potentially important implications for the distribution of tracers in the oceans; these effects need to be parameterized in non-eddy-resolving numerical models. Finally, this study explores the roles of eddies in sustaining the jets in a quasi-steady state. The jet formation is described in detail by BKPa in an idealized QG model of oceanic flow, as a multistage process governed by baroclinic instability. The relationship of the BKPa mechanism to the GCM simulation described in this manuscript will be a topic of future studies.

APPENDIX

Balance of Terms in the Potential Vorticity Equation

a. Potential vorticity

We first consider the full potential vorticity:

$$q = (\nabla \times \mathbf{u} + f\mathbf{k}) \cdot \nabla\rho = f\frac{\partial\rho}{\partial z} + \left(\frac{\partial w}{\partial y} - \frac{\partial v}{\partial z}\right)\frac{\partial\rho}{\partial x}$$
$$+ \left(\frac{\partial u}{\partial z} - \frac{\partial w}{\partial x}\right)\frac{\partial\rho}{\partial y} + \left(\frac{\partial v}{\partial x} - \frac{\partial u}{\partial y}\right)\frac{\partial\rho}{\partial z}. \quad \text{(A1)}$$

The second and third terms on the right-hand side of (A1) are traditionally neglected for large-scale oceanic flows. Here, we demonstrate that these terms are small even on the meridional scale of the jets. The slope of the isopycnals, $\alpha = \partial\rho/\partial y(\partial\rho/\partial z)^{-1}$, for nearly QG motions can be assumed to be $O[(U/fL)(f^2L^2/N^2D^2)(D/L)]$ (Pedlosky 1987); the slope of the isotachs $\partial u/\partial y(\partial u/\partial z)^{-1}$ can be scaled by the aspect ratio . In these expressions, U is the scale for horizontal velocity, L is the meridional scale, D is the vertical scale, and N is the Brünt–Väisälä frequency. It is then easy to see that $\partial u/\partial z(\partial\rho/\partial y) \ll \partial u/\partial y(\partial\rho/\partial z)$, which can be further verified using our estimates from the model: 2–5×10^{-4} for the isopycnal slope and 2.5–5×10^{-3} for D/L. Since the terms involving vertical velocities are small—$(\partial w/\partial x, \partial w/\partial y) \ll z(\partial u/\partial x, \partial v/\partial z)$—we arrive at the following approximation to (A1):

$$q \approx (f + \zeta)\frac{\partial\rho}{\partial z}. \quad \text{(A2)}$$

The relative vorticity in (A2) is expected to be important on the horizontal scales, characteristic for quasi-geostrophic motions on the beta plane, $L^2 \sim U/(df/dy)$, or approximately 100 km. On the meridional scales of several degrees, the relative vorticity can be neglected in (A2) unless the derivatives in PV are analyzed (as in the PV balance discussed below).

b. PV tendency terms

After splitting the velocities and density into the time-mean and eddy parts and averaging the PV equation in time, the left-hand side of the Eq. (12) becomes

$$\overline{\mathbf{u} \cdot \nabla(f + \zeta)\frac{\partial \rho}{\partial z}} = \overline{\mathbf{u}' \cdot \nabla\left(\varsigma'\frac{\partial \overline{\rho}}{\partial z}\right)} + \overline{\overline{\mathbf{u}} \cdot \nabla\left(\overline{\varsigma}\frac{\partial \overline{\rho}}{\partial z}\right)}$$

$$+ \overline{\overline{\mathbf{u}} \cdot \nabla\left(f\frac{\partial \overline{\rho}}{\partial z}\right)} + \overline{\mathbf{u}' \cdot \nabla\left(f\frac{\partial \rho'}{\partial z}\right)}$$

$$+ \overline{\mathbf{u}' \cdot \nabla\left(\overline{\varsigma}\frac{\partial \rho'}{\partial z}\right)} + \overline{\mathbf{u}' \cdot \nabla\left(\varsigma'\frac{\partial \rho'}{\partial z}\right)}$$

$$+ \overline{\overline{\mathbf{u}} \cdot \nabla\left(\varsigma'\frac{\partial \rho'}{\partial z}\right)}, \qquad (A3)$$

where the last three terms are verified to be small compared to any of the first four terms.

The diabatic term on the right-hand side of (12) expands into

$$\overline{(\nabla \times \mathbf{u} + f\mathbf{k}) \cdot \nabla\left(\frac{\partial \rho}{\partial t} + \mathbf{u} \cdot \nabla \rho\right)}$$

$$= f\frac{\partial}{\partial z}\overline{(\mathbf{u} \cdot \nabla \rho)} + \overline{(\nabla \times \mathbf{u}) \cdot \nabla\left(\frac{\partial \rho}{\partial t} + \mathbf{u} \cdot \nabla \rho\right)}, \quad (A4)$$

where the second term on the right-hand side of (A4) is verified to be small compared to the first term. Let us now estimate the order of magnitude of the first term on the right-hand side of (A4). Using the equation for density, we obtain

$$f\frac{\partial}{\partial z}\overline{(\mathbf{u} \cdot \nabla \rho)} = f\frac{\partial}{\partial z}\overline{\Phi}_{\text{DIFF}}, \qquad (A5)$$

where Φ_{DIFF} stands for all diffusion terms. Expanding the left-hand side, and assuming that the diffusion terms on isopycnals are dominated by the vertical diffusion term $\partial[k_v(\partial \rho/\partial z)]/\partial z$ (a likely scenario in the real ocean), we obtain the following scaling estimate:

$$\frac{\partial \mathbf{u}}{\partial z} \cdot \nabla \rho + \mathbf{u} \cdot \nabla \frac{\partial \rho}{\partial z} \sim \frac{\partial^2}{\partial z^2}\left(k_v\frac{\partial \rho}{\partial z}\right). \qquad (A6)$$

The diabatic term [the sum of two terms on the left-hand side of (A6)] can, therefore, be scaled by the diffusion term on the right-hand side. The first term on the left-hand side is small compared to the second term. To see this, we split the total velocity into geostrophic $\mathbf{u}_g$ and ageostrophic $\mathbf{u}_a$ parts: $\mathbf{u} = \mathbf{u}_g + \mathbf{u}_a$. Following an assumption of quasigeostrophy, which is expected to be valid on the scale of the jets, we assume that the ratio between these two velocity components is given by the Rossby number and is small: $\mathbf{u}_a/\mathbf{u}_g \sim U/fL \ll 1$. Taking into account a thermal wind balance, the first term on the left-hand side of (A6) becomes

$$\frac{\partial \mathbf{u}}{\partial z} \cdot \nabla \rho = \frac{\partial \mathbf{u}_a}{\partial z} \cdot \nabla \rho \sim \frac{U^2}{fDL^2}\delta\rho, \qquad (A7)$$

where $\delta\rho$ is the density anomaly. The second term on the left-hand side of (A6), the form stress forcing, scales as $\mathbf{u} \cdot \nabla(\partial \rho/\partial z) \sim (U/DL)\delta\rho$ and, therefore, tends to dominate the entire diabatic term. Its ratio to the diffusion term can be scaled as $\alpha UD/k_v \sim U^2f/N^2k_v$.

REFERENCES

Andrews, D. G., and M. E. McIntyre, 1976: Planetary waves in horizontal and vertical shear: The generalized Eliassen–Palm relation and the mean zonal acceleration. *J. Atmos. Sci.,* **33,** 2031–2048.

Baldwin, M., P. Rhines, H.-P. Huang, and M. McIntyre, 2007: The jet-stream conundrum. *Science,* **315,** 467–468.

Berloff, P., 2005a: On rectification of randomly forced flows. *J. Mar. Res.,* **63,** 497–527.

——, 2005b: On dynamically consistent eddy fluxes. *Dyn. Atmos. Oceans,* **38,** 123–146.

——, I. Kamenkovich, and J. Pedlosky, 2009a: A mechanism for the formation of multiple zonal jets in the oceans. *J. Fluid Mech.,* in press.

——, ——, and ——, 2009b: A model of multiple zonal jets in the oceans: Dynamical and kinematical analysis. *J. Phys. Oceanogr.,* in press.

Booth, J., and I. Kamenkovich, 2008: Isolating the role of transient mesoscale eddies in mixing of a passive tracer in an eddy resolving model. *J. Geophys. Res.,* **113,** C05021, doi:10.1029/2007JC004510.

Boyer, T., S. Levitus, H. Garcia, R. Locarnini, C. Stephens, and J. Antonov, 2005: Objective analyses of annual, seasonal, and monthly temperature and salinity for the World Ocean on a 0.25 degree grid. *Int. J. Climatol.,* **25,** 931–945.

Danilov, S., and V. Gryanik, 2004: Barotropic beta-plane turbulence in a regime with strong zonal jets revisited. *J. Atmos. Sci.,* **61,** 2283–2295.

——, and D. Gurarie, 2004: Scaling, spectra and zonal jets in beta-plane turbulence. *Phys. Fluids,* **16,** 2592–2603.

Dritschel, D., and M. E. McIntyre, 2008: Multiple jets as PV staircases: The Phillips effect and resilience of eddy-transport barriers. *J. Atmos. Sci.,* **65,** 855–874.

Galperin, B., H. Nakano, H. Huang, and S. Sukoriansky, 2004: The ubiquitous zonal jets in the atmospheres of giant planets and Earth's oceans. *Geophys. Res. Lett.,* **31,** L13303, doi:10.1029/2004GL019691.

Gnanadesikan, A., 1999: A simple predictive model for the structure of the oceanic pycnocline. *Science,* **283,** 2077–2079.

Griffies, S. M., and R. Hallberg, 2000: Biharmonic friction with a Smagorinsky-like viscosity for use in large-scale eddy-permitting ocean models. *Mon. Wea. Rev.,* **128,** 2935–2946.

Henning, C. C., and G. Vallis, 2004: The effects of mesoscale eddies on the main subtropical thermocline. *J. Phys. Oceanogr.,* **34,** 2428–2443.

Hogg, N., and B. Owens, 1999: Direct measurement of deep circulation within the Brazil basin. *Deep-Sea Res.,* **46,** 335–353.

Huang, H.-P., and W. Robinson, 1998: Two-dimensional turbulence and persistent zonal jets in a global barotropic model. *J. Atmos. Sci.,* **55,** 611–632.

——, A. Kaplan, E. Curchitser, and N. Maximenko, 2007: The degree of anisotropy for mid-ocean currents from satellite observations and an eddy-permitting model simulation. *J. Geophys. Res.,* **112,** C09005, doi:10.1029/2007JC004105.

Kramer, W., M. van Buren, H. Clercx, and G. van Heijst, 2006: β-plane turbulence in a basin with no-slip boundaries. *Phys. Fluids,* **18,** 026603, doi:10.1063/1.2173285.

LaCasce, J., and J. Pedlosky, 2004: The instability of Rossby basin modes and the oceanic eddy field. *J. Phys. Oceanogr.,* **34,** 2027–2041.

Ledwell, J. R., A. J. Watson, and C. S. Law, 1993: Evidence for slow mixing across the pycnocline from an open-ocean tracer-release experiment. *Nature,* **364,** 701–703.

Masumoto, Y., and Coauthors, 2004: A fifty-year eddy-resolving simulation of the world ocean—Preliminary outcomes of OFES (OGCM for the Earth Simulator). *J. Earth Simul.,* **1,** 35–56.

Maximenko, N., B. Bang, and H. Sasaki, 2005: Observational evidence of alternating zonal jets in the world ocean. *Geophys. Res. Lett.,* **32,** L12607, doi:10.1029/2005GL022728.

Nadiga, B., 2006: On zonal jets in oceans. *Geophys. Res. Lett.,* **33,** L10601, doi:10.1029/2006GL025865.

Nakamura, M., and Y. Chao, 2000: On the eddy isopycnal thickness diffusivity of the Gent–McWilliams subgrid mixing parameterization. *J. Climate,* **13,** 502–510.

——, and T. Kagimoto, 2006: Potential vorticity and eddy potential enstrophy in the North Atlantic Ocean simulated by a global eddy-resolving model. *Dyn. Atmos. Oceans.,* **41,** 28–59.

Nakano, H., and H. Hasumi, 2005: A series of zonal jets embedded in the broad zonal flows in the Pacific obtained in eddy-permitting ocean general circulation models. *J. Phys. Oceanogr.,* **35,** 474–488.

Nowlin, W., and J. Klinck, 1986: The physics of the Antarctic Circumpolar Current. *Rev. Geophys.,* **24,** 469–491.

Ollitrault, M., M. Lankhorst, D. Fratantoni, P. Richardson, and W. Zenk, 2006: Zonal intermediate currents in the equatorial Atlantic Ocean. *Geophys. Res. Lett.,* **33,** L05605, doi:10.1029/2005GL025368.

Orsi, A. H., T. Whitworth, and W. Nowlin, 1995: On the meridional extent and fronts of the Antarctic Circumpolar Current. *Deep-Sea Res. I,* **42,** 641–673.

Pacanowski, R. C., and S. M. Griffies, 1999: The MOM 3 manual. GFDL Tech. Rep. 4, 680 pp.

Panetta, R. L., 1993: Zonal jets in wide baroclinically unstable regions: Persistence and scale selection. *J. Atmos. Sci.,* **50,** 2073–2106.

Pedlosky, J., 1987: *Geophysical Fluid Dynamics*. 2nd ed. Springer-Verlag, 710 pp.

Rhines, P., 1994: Jets. *Chaos,* **4,** 313–339.

——, 1975: Waves and turbulence on a beta-plane. *J. Fluid Mech.,* **69,** 417–443.

Richards, K., N. Maximenko, F. Bryan, and H. Sasaki, 2006: Zonal jets in the Pacific Ocean. *Geophys. Res. Lett.,* **33,** L03605, doi:10.1029/2005GL024645.

Sokolov, S., and S. Rintoul, 2007: Multiple jets of the Antarctic Circumpolar Current south of Australia. *J. Phys. Oceanogr.,* **37,** 1394–1412.

Smith, K. S., and G. K. Vallis, 2001: The scales and equilibration of midocean eddies: Freely evolving flow. *J. Phys. Oceanogr.,* **31,** 554–571.

——, and ——, 2002: The scales and equilibration of midocean eddies: Forced-dissipative flow. *J. Phys. Oceanogr.,* **32,** 1699–1720.

Smith, R. D., M. E. Maltrud, F. O. Bryan, and M. W. Hecht, 2000: Numerical simulation of the North Atlantic Ocean at 1/10°. *J. Phys. Oceanogr.,* **30,** 1532–1561.

Talley, L. D., 2003: Shallow, intermediate, and deep overturning components of the global heat budget. *J. Phys. Oceanogr.,* **33,** 530–560.

Thompson, A., and W. Young, 2007: Two-layer baroclinic eddy heat fluxes: Zonal flows and energy balance. *J. Atmos. Sci.,* **64,** 3214–3231.

Treguier, A., and R. L. Panetta, 1994: Multiple zonal jets in a quasigeostrophic model of the Antarctic Circumpolar Current. *J. Phys. Oceanogr.,* **24,** 2263–2277.

——, N. Hogg, M. E. Maltrud, K. Speer, and V. Thierry, 2003: The origin of deep zonal flows in the Brazil basin. *J. Phys. Oceanogr.,* **33,** 580–599.

Vallis, G. K., 2006: *Atmospheric and Oceanic Fluid Dynamics*. Cambridge University Press, 745 pp.

——, and M. E. Maltrud, 1993: Generation of mean flows and jets on a beta plane and over topography. *J. Phys. Oceanogr.,* **23,** 1346–1362.